



Contents lists available at ScienceDirect

Arabian Journal of Chemistry

journal homepage: www.ksu.edu.sa

Systems pharmacology-based dissection of potential mechanisms of *Exocarpium Citri Grandis* for the treatment of chronic bronchitis

Jiawen Huang^{a,1}, Zaibin Xu^{a,1}, Jiayu Li^a, Xinqian He^b, Xinan Huang^b, Xiaoling Shen^{a,*}, Zhuohui Luo^{c,d,e,*}

^a Science and Technology Innovation Center, Guangzhou University of Chinese Medicine, Guangzhou 510405, China

^b Artemisinin Research Center, Guangzhou University of Chinese Medicine, Guangzhou 510422, China

^c Honz Pharmaceutical Co., Ltd., Haikou 570311, China

^d Hainan Pharmaceutical Research and Development Science Park, Haikou 571199, China

^e Research Center for Drug Safety Evaluation of Hainan Province, Hainan Medical University, Haikou 571199, China

ARTICLE INFO

Keywords:

Exocarpium Citri Grandis

Chronic bronchitis

Network pharmacology

Molecular docking

Molecular dynamics simulation

Transcriptomics

ABSTRACT

Exocarpium Citri Grandis (ECG), a precious traditional Chinese medicine (TCM), has been widely utilized to improve the symptoms of chronic bronchitis (CB) such as cough or sputum. However, its underlying pharmacological mechanisms remain unclear. To investigate the potential mechanisms of ECG for the treatment of CB, a comprehensive systems pharmacology strategy combining network pharmacology, molecular docking, molecular dynamics simulations, and molecular biology experiments *in vitro* was carried out. In this study, 46 potential targets of CB screened for 10 active ingredients of ECG were strongly linked to inflammatory responses, immune processes, and apoptosis. Molecular docking revealed that the active ingredients of ECG have high binding activity for MyD88, NF- κ B p65, Caspase9, and Caspase3, respectively. Meanwhile, MD simulations confirmed that neohesperidin and naringenin have high stability and low binding free energy with NF- κ B p65 and Caspase3 in the binding pocket. In the LPS-induced RAW264.7 cell inflammatory model, ECG markedly reduced the secretion of IL1 β , IL6, TNF- α , and NO. Transcriptomics showed a total of 337 differential expression genes (DEGs) were screened after ECG treatment, of which 233 down-regulated DEGs were closely associated with the NF- κ B signaling pathway, the Toll-like receptor signaling pathway, the IL-17 signaling pathway, and the TNF signaling pathway. Further analysis results revealed that ECG significantly down-regulated the expression of TLR4, MyD88, NF- κ B p65, NF- κ B p-p65 (S536), p-I κ B α (S36), COX2, ICAM1, and iNOS, and up-regulated the expression of I κ B α , inhibited NF- κ B p65 entry into the nucleus, thereby suppressing NF- κ B signaling transduction. Furthermore, ECG also significantly up-regulated the expression of Bcl-2 and down-regulated the expression of Bax, Caspase3, Caspase8, and Caspase9, inhibiting apoptosis in a dose-dependent manner. Our study reveals the potential pharmacological mechanisms of ECG for the treatment of CB and provides a scientific basis for its clinical application.

1. Introduction

Chronic bronchitis (CB) is a common disease caused by chronic non-specific inflammation of the trachea, bronchial mucosa, and

surrounding tissues mainly resulting from infectious or non-infectious factors (Malesker et al., 2020). The pathology of CB is characterized by hyperplasia of bronchial glands, increased mucus secretion, and the clinical presence of symptoms like cough, sputum, or shortness of breath

Abbreviations: CB, Chronic bronchitis; CCK8, Cell Counting Kit 8; DEGs, Differential expression genes; DL, Drug-likeness; ECG, *Exocarpium Citri Grandis*; FBS, Fetal bovine serum; GO, Gene Ontology; KEGG, Kyoto Encyclopedia of Genes and Genomes; MD, Molecular dynamics; MyD88, Myeloid differentiation factor 88; NF- κ B, Nuclear factor κ B; NO, Nitric oxide; OB, Oral bioavailability; PI, Propidium iodide; PME, Particle Mesh Ewald; RMSD, Root mean square deviation; SASA, Solvent-accessible surface area; TCM, Traditional Chinese medicine; TCMSP, Traditional Chinese Medicine System Pharmacology; TLR4, Toll-like receptor 4.

Peer review under responsibility of King Saud University.

* Corresponding authors.

E-mail addresses: xshen2@gzucm.edu.cn (X. Shen), zhuohuiluo@126.com (Z. Luo).

¹ These authors contributed equally to this work.

<https://doi.org/10.1016/j.arabjc.2023.105428>

Received 20 July 2023; Accepted 1 November 2023

Available online 2 November 2023

1878-5352/© 2023 The Author(s). Published by Elsevier B.V. on behalf of King Saud University. This is an open access article under the CC BY-NC-ND license (<http://creativecommons.org/licenses/by-nc-nd/4.0/>).

that last for more than two consecutive years and every three months is the gold standard for defining CB (Anonymou, 1965). CB is a long-term inflammation of the bronchi that has a highly complex etiology. Cigarette smoking is a common well-established risk factor (Pelkonen et al., 2006). As research progresses, more exposures are being elucidated in recent years (Kim and Criner, 2013).

Traditional Chinese medicine (TCM) is a medical discipline that was formed and evolved in the daily lives of the Chinese people, and in the process of their fight against diseases over thousands of years, sayings like “Shennong (Celestial Farmer) tasting a hundred herbs” theory are characteristic. *Exocarpium Citri Grandis* (ECG, Huajuhong in Chinese) is the dried unripe or almost ripe peel of *Citrus grandis* ‘Tomentosa’ or *Citrus grandis* (L.) Osbeck (Fam. Rutaceae) is mainly produced in Huazhou City of Guangdong Province. It is an indication product of Chinese National Geography and an authentic Chinese medicinal material of food and medicine from the same source, known as southern ginseng. Chemical studies have shown that ECG mainly contains flavonoid, coumarin, and volatile oil components (Liu et al., 2022; Kong et al., 2022) with pharmacological effects such as promoting the discharge of gas, secretion of gastric acid, dispelling phlegm, stopping cough, anti-inflammatory, and preventing platelet aggregation (Li et al., 2006; Zhu et al., 2019, Zhong et al., 2021), which has been used to treat chronic bronchitis for many years (Chen and Lin, 2004; Jiang et al., 2014). Indeed, ECG is a monarch medicine in many famous TCM prescriptions, such as “Juhong Pills” and “Juhong Capsules”. Accumulating clinical evidence indicates that “Juhong Pills” and “Juhong Capsules” are effective in treating patients with chronic bronchitis and improving clinical symptoms (Jiang et al., 1994; Xie et al., 2022). However, the molecular pharmacological mechanisms of ECG in treating CB remain unclear.

Network pharmacology is a new interdisciplinary subject that uses artificial intelligence and big data to conduct systematic research (Hopkins, 2007). It has gradually evolved into an integrated approach to explore the pharmacological mechanisms of Chinese medicine or Chinese medicine based on a complex system in collaboration with computerized molecular docking and molecular dynamics simulation techniques (Liu et al., 2020; Luo et al., 2022), which provides new scientific and technological support for the rational clinical drugs use and drug development.

In this study, a network pharmacology approach was used to predict the targets of ECG for the treatment of CB, which was then virtually validated using computerized molecular docking and molecular dynamics simulation, followed by an LPS-induced inflammation model with transcriptomics and other experimental approaches to further elucidate the significant anti-inflammatory capacity of ECG. Our research provides a modern scientific basis for the use of ECG in CB therapy.

2. Materials and methods

2.1. Chemicals and reagents

Lipopolysaccharide (LPS) was supplied from Sigma-Aldrich Co. (Shanghai, China). Cell Counting Kit 8 (CCK-8) was purchased from Dojindo Laboratory (Kumamoto, Japan). Fetal bovine serum (FBS) and RPMI 1640 medium were provided by Biological Industries (Kibbutz Beit Haemek, Israel). Information about the antibodies used for immunoblotting is shown in Supplementary Table 1. Unless otherwise noted, all other chemicals were supplied by Sigma-Aldrich.

2.2. Establishment of the “ECG-ingredients-targets” interactions

To construct a network diagram of ECG-ingredients-targets interactions, two suggested drug screening criteria of TCMSP (<https://tcmssp.com/tcmssp.php>) database (Ru et al., 2014) such as oral bioavailability (OB) threshold $\geq 30\%$ and drug-likeness (DL) threshold

≥ 0.18 , were used to screen the active ingredients and their related targets in ECG. Then, Cytoscape software (Version: 3.6.0) was used to establish a network diagram of “ECG-ingredients-targets” interactions.

2.3. Targets screening for ECG treatment of CB

To obtain CB-related targets, the Drugbank (<https://www.drugbank.ca/>) (Wishart et al., 2008), Genecards (<https://www.genecards.org/>) (Rebhan et al., 1997), OMIM (<https://omim.org/>) (Amberger et al., 2015), and DigSee (<http://210.107.182.61/geneSearch/>) (Kim et al., 2013) databases were used to screen via searching “Chronic bronchitis” as the keyword. Subsequently, overlapping targets were obtained by screening with ECG active ingredients-related targets from TCMSP, and recognized as potential targets for ECG treatment of CB.

2.4. Construction of a protein–protein interaction network

The screened overlapping proteins were subjected to analysis using the STRING (Version: 11.5) data resources (<https://cn.string-db.org/>) (Szklarczyk et al., 2017), and then the tsv. format was exported to Cytoscape for construction and visualization of the protein–protein interaction (PPI) network.

2.5. Biological functional enrichment analysis

To further reveal the biological function of the overlapping target, the Gene Ontology (GO) enrichment and Kyoto Encyclopedia of Genes and Genomes (KEGG) pathway analysis was performed using DAVID bioinformatics resources (<https://david.ncifcrf.gov/>) (Huang et al., 2009), a comprehensive set of functional annotation tools to find out the biological function and molecular pathways of the selected targets.

2.6. Molecular docking

Molecular docking of ECG active ingredients to targets was analyzed as previously described (Luo et al., 2022; Liu et al., 2018; Xie et al., 2019). Briefly, the structures of ECG active ingredients were retrieved from the PubChem database (<https://pubchem.ncbi.nlm.nih.gov/>) (Wang et al., 2009) and optimized using molecular mechanics to obtain the most stable systems. The RCSB PDB database was then used to retrieve the 3D crystal structure of each target (<https://www.rcsb.org/>) (Burley et al., 2019) and processed for structural correction. Molecular docking of active ingredients and targets were analyzed using SYBYL-X 2.2.1 software. The docking mode was set as Suflex-Dock Geom (SFXC), and then the protein was subjected to Hydrogenation and Charging, as well as Protomol Generation for Multi-channel Surface to obtain SFXC files. Next, fully flexible docking was selected for optimal docking conformation. Finally, active ingredients-proteins binding pattern schematization and related binding amino acids were analyzed using Discover Studio Visualizer 2016. The box sizes for molecular docking targets are shown in Supplementary Table 2.

2.7. Molecular dynamics simulation

To further investigate the stability of ECG active ingredients with key targets of CB in the binding pocket. Molecular dynamics (MD) simulations of 100 ns were done using the GROMACS v.2020.4 software package as previously described (Luo et al., 2022). Briefly, the crystal structures of nuclear factor κ B (NF- κ B) p65 (PDB_ID: 5URN) and Caspase3 (PDB_ID: 5IAE) proteins were obtained from the PDB bank. The molecular structures of the small molecules were retrieved from the PubChem database (Wang et al., 2009). To eliminate close contact between atoms, energy minimization of proteins using the steepest descent method. Energy optimization of small molecule structures using Chem3D16 and molecular docking was done by SYBYL-X 2.2.1 software. MD simulations were run with constant temperature, pressure, and

periodic boundary conditions. The amber99sb-ildn force field and the TIP3P water model were used. The *acpype.py* script in AmberTools generates the force field parameters for small molecules. During the MD simulation, the LINCS technique with a 2.0 fs integration time step was used to limit hydrogen bonding. The Particle Mesh Ewald (PME) technique was used to compute the electrostatic interactions with a truncation value of 1.2 nm and the non-bonding interactions truncation value of 10 Å and every ten steps updated. All the MD simulations were run using the Berendsen method and V-rescale temperature coupling at constant temperatures of 300 K and 1 bar, respectively. Then, 100 ps of NVT and NPT equilibrium simulations at 300 K, followed by 100 ns of molecular dynamics simulations. For the protein–ligand complexes, a 100 ns MD simulation was completed. The binding free energy of complexes was determined using *g_mmpbsa* (Kumari et al., 2014). The output of the MD simulation was visualized using the software-embedded programs of GROMACS and Discover Studio Visualizer 2016.

2.8. ECG preparation

ECG herbal medicine (Batch No.: Z46-20220901), a monarch medicine in “Zhike Juhong Granules” prescriptions produced by Honz Pharmaceutical Co., Ltd. In the current study, the herb of ECG (100.1 g) was refluxed for 1 h in an 8-fold mixture of 50 % ethanol and water (v/v). After filtering through gauze, labeled as filtrate 1. Then the residue was refluxed with a 6-fold mixture of 50 % ethanol and water (v/v) for a further hour and also filtered through gauze, labeled as filtrate 2. Next, filtrate 1 and filtrate 2 were combined and concentrated. The concentrate was lyophilized at the end with a yield of 41.61 %, and the lyophilized sample was further analyzed by UPLC-Q/TOF-MS/MS (Supplementary Fig. 1).

2.9. Culture of cell

RAW264.7 Cells were cultured in RPMI 1640 medium (with 100 U/mL of penicillin, 100 µg/mL of streptomycin, and 10 % FBS) and incubated in a wet incubator at 37 °C with 5 % CO₂. Cells should be seeded onto culture dishes or plates for 24 h before performing all experiments. Cells were pre-treated with different concentrations of ECG (25, 50, 100 µg/mL) for 1 h and then exposed to 0.5 µg/mL LPS. After 24 h, the cells or the cell culture medium were then collected for subsequent analyses.

2.10. Cell viability assay

To determine the effect of ECG on cell viability, 2×10^4 cells per well were added to the 96-well plate. After 24 h, cells were treated with various concentrations of ECG for 24 h, and the blank group of cells was added with the same amount of complete culture medium. Finally, cell viability was assessed according to CCK-8 assay requirements.

2.11. Griess assay

The cell culture medium level of nitric oxide (NO) produced by cells was measured according to the instructions of the NO kit (Beyotime Biotechnology, China, S0021S).

2.12. Measurement of IL1β, IL6 and TNF-α

IL1β, IL6, and TNF-α levels in cell culture medium were measured according to the instructions of commercial kits (eBioscience, USA, 88-7013A-86, 88-7064-86, 88-7324-86).

2.13. RNA sequencing

Total RNA was extracted from cells with Trizol reagent and reversed transcribed into cDNA, followed by PCR amplification and purification to obtain PCR products for transcriptomics as previously described (Li

et al., 2020), Quantification and detection were performed using a Qubit2.0 Fluorometer and Agilent 2100 bioanalyzer to detect libraries. The Illumina NovaSeq 6000 platform was used to sequence and generate 150 bp paired-end reads for subsequent high-quality analysis. Indexes of the reference genome were constructed using HISAT2 (v2.0.5) and compared to the reference genome. Read mapped to each gene was calculated by featureCounts (1.5.0-p3) for the FPKM of each gene. Differential expression genes (DGEs) between groups were identified using DESeq2 software (1.20.0) and the resulting *p* values (padj) were adjusted by Benjamini and Hochberg’s method to control the false discovery rate. GO enrichment analysis and KEGG pathway analysis of DGEs were performed respectively using clusterProfiler (3.8.1) software.

2.14. Immunofluorescence

Cells were perforated with 0.5 % Triton X-100 at room temperature for 20 min after being fixed with 4 % paraformaldehyde for 15 min. Then, cells were blocked by 5 % BSA solution for 1 h, incubated by NF-κB p65 antibody (1: 100) overnight at 4 °C. After being washed, cells were incubated by fluorescent secondary antibody (1: 1000) for 1 h at room temperature. Finally, cells were covered by an antifade mounting medium containing DAPI. Pictures were observed under a fluorescence microscope (Nikon, Shanghai, China).

2.15. Apoptosis assay

Cells were collected and stained with Annexin V-FITC and propidium iodide (PI) following the instructions of the Annexin V-FITC apoptosis detection kit (Beyotime Biotechnology, China, C1062L). Images were observed by fluorescence microscope (Leica, Wetzlar, Germany).

2.16. Western blot

Protein samples were extracted from cells after treatment, and their concentrations were measured by a BCA kit (Beyotime Biotechnology, China, P0010). Proteins were separated by 10 % SDS-polyacrylamide gel and transferred to PVDF membranes. The membranes were then incubated with different primary antibodies overnight at 4 °C, and followed by a secondary antibody. ECL kit (Guangdong Prochem Biotechnology Co.,Ltd. China, ECL-0102) was used and images were obtained using Molecular Imager® (BIO-RAD, CA, United States).

2.17. Statistical analysis

The values were expressed as the mean ± SD and analyzed using GraphPad Prism 6.0 (San Diego, CA, USA). The significance of the differences was analyzed using a one-way ANOVA followed by Bonferroni’s multiple comparisons test. *P* < 0.05 was considered statistically significant.

3. Results

3.1. Construction of a “ECG-ingredients-targets” network

To obtain the active ingredients of ECG, the TCMSP database was used for screening. In this study, 10 active ingredients were recognized (Supplementary Table 3), and 99 potential targets were predicted. As shown in Fig. 1, the ECG-active ingredients-related targets network was constructed.

3.2. PPI network construction

The active ingredients-related targets of ECG may be closely associated with CB-related targets obtained from Drugbank, Genecards, OMIM, and DigSee databases. To further investigate the underlying

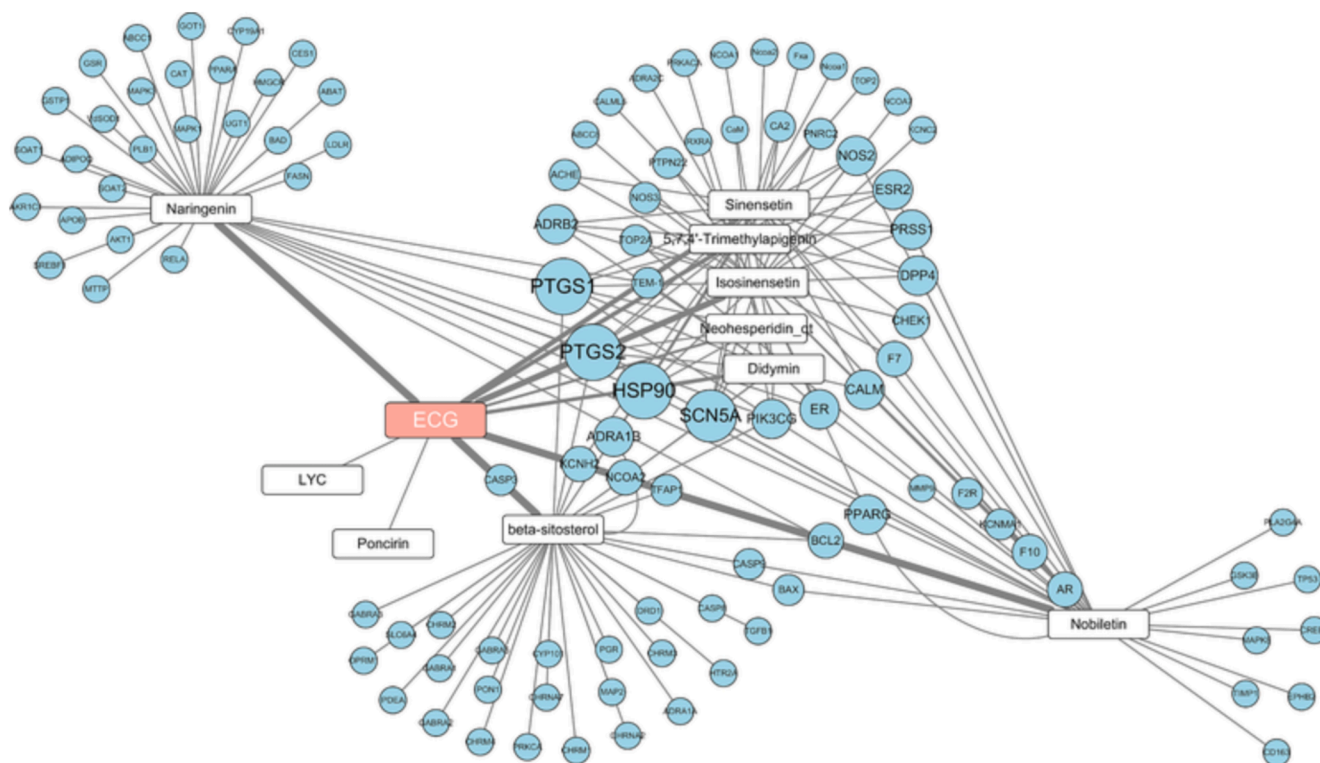


Fig. 1. Network pharmacology predicted the active ingredients-targets interactions for ECG. (Nodes with orange, white, and blue represent ECG, ingredients, and targets, respectively.). (For interpretation of the references to colour in this figure legend, the reader is referred to the web version of this article.)

pharmacological effects of ECG on CB, a Venn diagram was utilized to visualize the correlation. As shown in Fig. 2A, 46 overlapping targets were screened, and their interactions were analyzed through STRING data resource. Then, the PPI network was constructed through Cytoscape software and presented 46 nodes and 1204 edges. Among them, AKT1 (degree = 42), MAPK3 (degree = 41), PTGS2 (degree = 39), CASP3 (degree = 38), NOS3 (degree = 34), MAPK1 (degree = 34), PTGS1 (degree = 33), MAPK8 (degree = 32), PIK3CG (degree = 31) and RELA (degree = 30) with a higher degree were most likely involved in the inflammations and pathogenesis processes of CB (Fig. 2B).

3.3. GO and KEGG pathway enrichment analysis

In the present study, GO enrichment analysis based on DAVID bioinformatics resources revealed that overlapping targets were involved in

response to the drug, adenylate cyclase-inhibiting G-protein coupled acetylcholine receptor, positive regulation of apoptotic process, response to lipopolysaccharide, cellular response to reactive oxygen species, negative regulation of the apoptotic process, G-protein coupled acetylcholine receptor in biological processes (Fig. 3A). Enzyme binding, protein homodimerization activity, G-protein coupled serotonin receptor activity, ubiquitin protein ligase binding, protease binding, NADP binding, transcription coactivator binding, histone deacetylase binding, protein serine/threonine kinase activity, MAP kinase activity, enzyme binding, protein homodimerization activity in molecular functions (Fig. 3B). Plasma membrane, synapse, macromolecular complex, cytoplasm, cytosol, Golgi apparatus, mitochondrion, nucleus, nucleoplasm, endoplasmic reticulum in cellular components (Fig. 3C), suggesting that ECG may play a pharmacological role in treating CB through these biological functions.

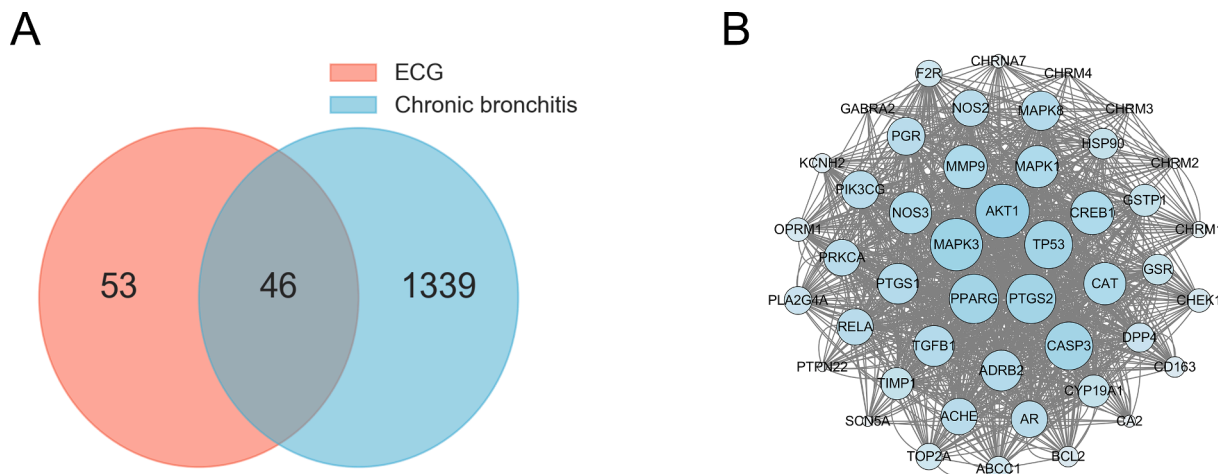


Fig. 2. Venn diagram of ECG and CB-related targets (A), PPI network of potential targets (B).

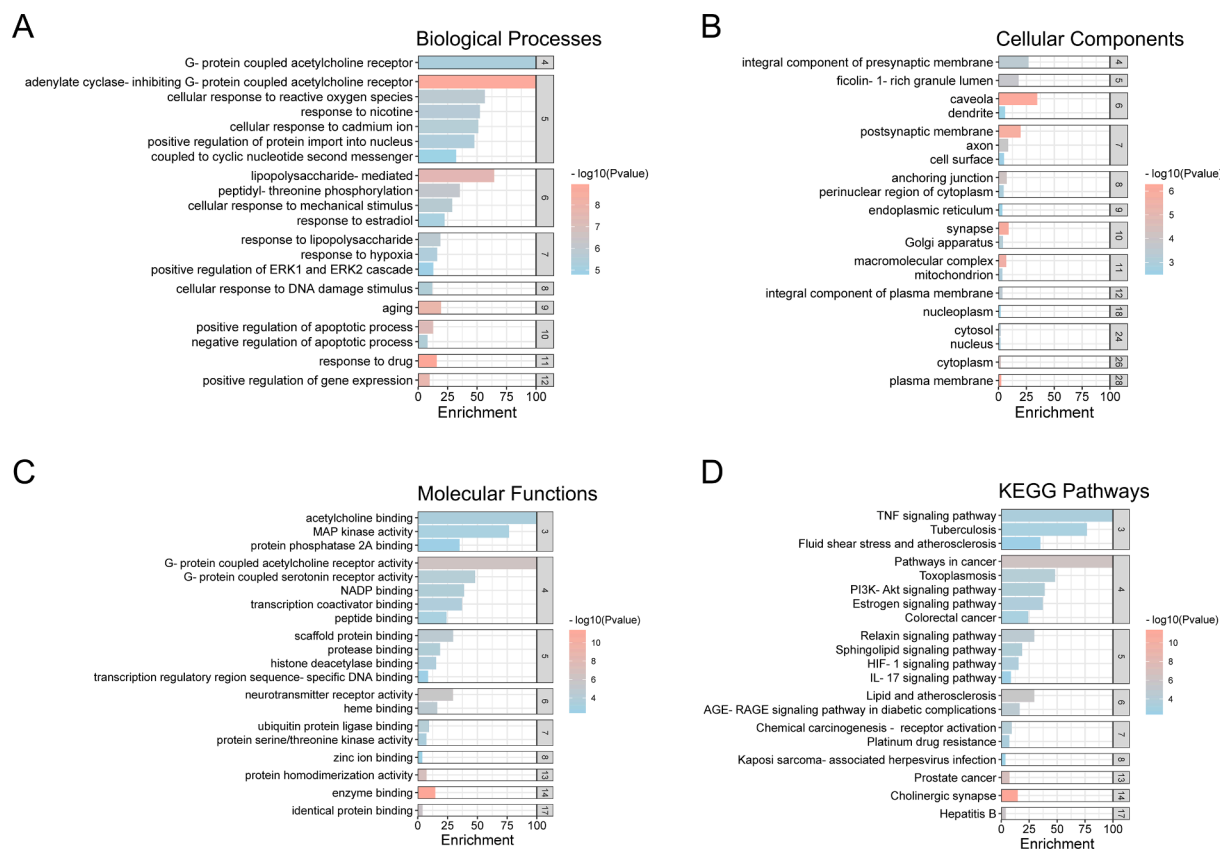


Fig. 3. GO enrichment and KEGG pathways analysis of the anti-CB targets of ECG. (A) Biological Processes, (B) Cellular Components, (C) Molecular Function, (D) KEGG Pathway.

Furthermore, KEGG pathway enrichment analysis revealed the TNF signaling pathway, the IL-17 signaling pathway, and the PI3K-Akt signaling pathway may be remarkably related to the pathogenesis of CB, indicating that ECG can act as a therapeutic CB by ameliorating the inflammatory response that is closely linked to these pathways (Fig. 3D and Supplementary Table 4).

3.4. Interactions between active ingredients with targets

The above network pharmacology analysis highlighted the important role of ECG active ingredients in anti-inflammatory effects. Chemical studies showed that naringin, naringenin, and neohesperidin were highly abundant in ECG herbal medicine (Liu et al., 2022; Kong et al., 2022; Jiang et al., 2014). In this study, the experimental ECG sample was also examined by UPLC-Q/TOF-MS/MS technology. As expected, naringin, naringenin, and neohesperidin were identified (Supplementary Fig. 1, Supplementary Fig. 2, and Supplementary Table 5). Based on the results above, the screened active ingredients with key targets of CB inflammatory signaling, such as myeloid differentiation factor 88 (MyD88) and NF- κ B p65 (RelA), were investigated in the binding mode by molecular docking (Supplementary Table 6–9). An ingredient binding to the target with a total score > 7 and a C-score close to 5 indicates strong activity (Liu et al., 2018; Xie et al., 2019). The results showed that neohesperidin docking to MyD88 (PDB_ID: 4DOM) gave a total score and C-score of 9.2265 and 1, respectively (Supplementary Table 7). The binding modes were that neohesperidin formed hydrogen bonds with protein residues SER 209, SER 194, ILE 165, and ASP 195, formed carbon-hydrogen bonds with protein residues LYS 231, TYR 167, interacted with van der Waals forces with protein residues ILE 212, PHE 235, VAL 193, CYS 168, ILE 172, PHE 164, GLU 232, hydrophobic interactions in the form of π bond with protein residues PRO 169, VAL 198, and formed lone pair- π interaction with protein residue TYR 167

(Fig. 4A-C). Naringenin docking to MyD88 (PDB_ID: 7BER) gave a total score and C-score of 7.2349 and 0, respectively (Supplementary Table 7). The binding modes were that naringenin formed hydrogen bonds with protein residues SER 209, SER 194, ILE 165, and ASP 195, formed a carbon-hydrogen bond with protein residue ILE 253, interacted with van der Waals forces with protein residues THR 272, PRO 254, LEU 295, LEU 293, ARG 218, ARG 288, and hydrophobic interactions in the form of π bond with protein residues LYS 250, ILE 271 (Fig. 4D-F). Similarly, neohesperidin docking to NF- κ B p65 (PDB_ID: 5URN) gave a total score and C-score of 10.9476 and 2, respectively (Supplementary Table 9). The binding modes were that neohesperidin formed hydrogen bonds with protein residues GLU 10, MET 88, SER 535, LYS 11, MET 58, formed carbon-hydrogen bonds with protein residues ILE 8, PHE 9, HIS 87, ARG 86, MET 88, LYS 11, interacted with van der Waals forces with protein residues GLU 532, ASP 531, PHE 534, ILE 537, ASP 541, PHE 89, and hydrophobic interactions in the form of π bond with protein residues MET 59, LYS 57, ALA 538, MET 88 (Fig. 4G-I). Naringenin docking to NF- κ B p65 (PDB_ID: 5URN) gave a total score and C-score of 8.0717 and 2, respectively (Supplementary Table 9). The binding modes were that naringenin formed hydrogen bonds with protein residues MET 88, GLU 10, and ASP 531, formed a carbon-hydrogen bond with protein residue ASP 531, interacted with van der Waals forces with protein residues PHE 534, MET 59, SER 90, PHE 89, ILE 8, PHE 9, SER 535, GLU 532, GLY 530, hydrophobic interactions in the form of π bond with protein residue MET 88, and interacted with protein residue ASP 531 as a π -bond in a lone pair electron cloud (Fig. 4J-L).

In response to cellular stress, nucleolar translocation of NF- κ B p65 directly affects a nucleolar pathway/protein(s) to mediate apoptosis (Khandelwal et al., 2011). Caspases belonging to cysteinyl proteases, such as Caspase3, 8, and 9, were well-characterized roles in apoptosis and cytokine maturation. In the present study, neohesperidin binding with Caspase9 (PDB_ID: 1JXQ) provided a total score and C-score of

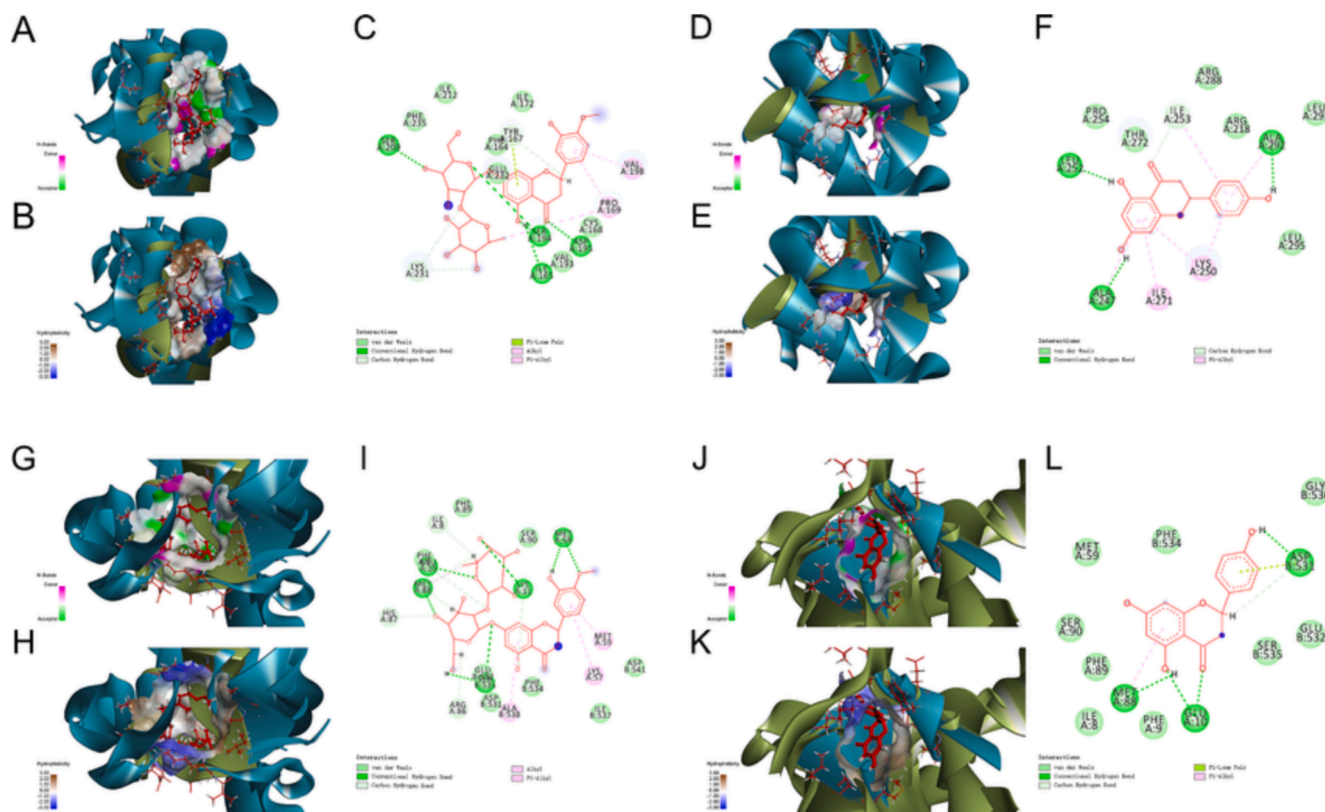


Fig. 4. Molecular docking analysis revealed the bond pattern of neohesperidin and naringenin with MyD88 and NF- κ B p65, respectively. (A-C) Molecular docking of neohesperidin and MyD88, (D-F) Molecular docking of naringenin and MyD88, (G-I) Molecular docking of neohesperidin and NF- κ B p65, (J-L) Molecular docking of naringenin and NF- κ B p65. (A, D, G, J): Areas of the donor and acceptor of hydrogen bond (H-bond). (B, E, H, K): Areas of hydrophobicity. (C, F, I, L): Two-dimensional patterns of the bond.

15.4065 and 2, respectively (Supplementary Table 11). The binding modes were that neohesperidin formed hydrogen bonds with protein residues PRO 271, SER 144, ASN 148, ASP 150, ASP 326, ARG 395, TYR 383, LEU 321, GLY 275, formed carbon-hydrogen bonds with protein residues GLY 274, PRO 271, SER 144, GLY 267, interacted with van der Waals forces with protein residues THR 268, ASN 266, PRO 322, THR 323, LYS 276, LEU 273, SER 272, GLY 147, LEU 145, ALA 149, SER 325, ILE 382, MET 386, SER 37, formed T-type interaction forces with protein residues TYR 383, GLY 267 at π - π bonds with amide bonds (Fig. 5A-C). Naringenin binding with Caspase9 (PDB_ID: 4RHW) provided a total score and C-score of 8.905 and 3, respectively (Supplementary Table 11). The binding modes were that naringenin formed hydrogen bonds with protein residues SER 23, LYS 21, ASP 53, PRO 47, GLN 57, formed carbon-hydrogen bonds with protein residues GLY 274, PRO 271, SER 144, GLY 267, interacted with van der Waals forces with protein residues THR 22, SER 48, ARG 52, hydrophobic interactions in the form of π bond with protein residues ARG 44, ALA 46, and forms an interaction force with protein residues GLY 47 via π -amide bond (Fig. 5D-F). Neohesperidin docking to Caspase3 (PDB_ID: 5IAE) provided a total score and C-score of 8.4479 and 4, respectively (Supplementary Table 13). The binding modes were that neohesperidin formed hydrogen bonds with protein residues TYR 197, LYS 137, and GLU 167, formed carbon-hydrogen bonds with protein residues GLY 125, TYR 195, GLU 124, interacted with van der Waals forces with protein residues PHE 266, GLY 202, ARG 164, TYR 197, LYS 137, LEU 136, TYR 195, THR 140, hydrophobic interactions in the form of π bond with protein residues TYR 105, PRO 201, PRO 201 (Fig. 5G-I). Naringenin docking to Caspase3 (PDB_ID: 5IAE) provided a total score and C-score of 7.9554 and 2, respectively (Supplementary Table 13). The binding modes were that naringenin formed hydrogen bonds with protein residues GLU 190, GLU 124, LYS 137, GLY 125, formed a carbon-hydrogen

bond with protein residue LYS 137, interacted with van der Waals forces with protein residues ALA 200, MET 268, PHE 266, ARG 164, ASP 135, TYR 197, ILE 160, THR 140, hydrophobic interactions in the form of π bond with protein residues PRO 201, LEU 136, and formed T-type interactions with protein residue TYR 195 through π - π bonds (Fig. 5J-L). Detailed information on the docking studies for other active ingredients was provided in Supplementary Table 10–13. All these results suggested that the ECG active ingredients could bind directly with MyD88, NF- κ B p65, Caspase3, and Caspase9, thereby inhibiting the inflammatory response and apoptosis to improve CB.

3.5. The dynamics stability simulation of active ingredients with targets

Research evidence has convincingly shown that the first line of protection against invading pathogens is innate immunity (Cameron et al., 2016). NF- κ B is a pleiotropic transcription factor involved in inflammatory and immune responses (Baeuerle and Henkel, 1994; Baeuerle and Baltimore, 1996). In the docking studies above, ECG active ingredients showed strong binding activity with the critical inflammatory target (RELA/p65). Thus, an MD simulation was carried out to further understand the binding pocket's stability. Root mean square deviation (RMSD) represents the sum of all atomic deviations of the conformation at a given moment from the target conformation, which is an essential measure of the system's stability. As shown in Fig. 6A, the neohesperidin-NF- κ B p65 system was in an equilibrium state from 30 to 100 ns with a mean RMSD value of 0.1168 ± 0.020 , and the RMSD values of the whole system converged, and the system reached equilibrium. In contrast, the naringenin-NF- κ B p65 system dramatically rose at 32 ns and then converged to equilibrium in the last 5 ns of time with a mean RMSD value of 0.1693 ± 0.017 . In addition, the variation of solvent-accessible surface area (SASA) with time showed that the more

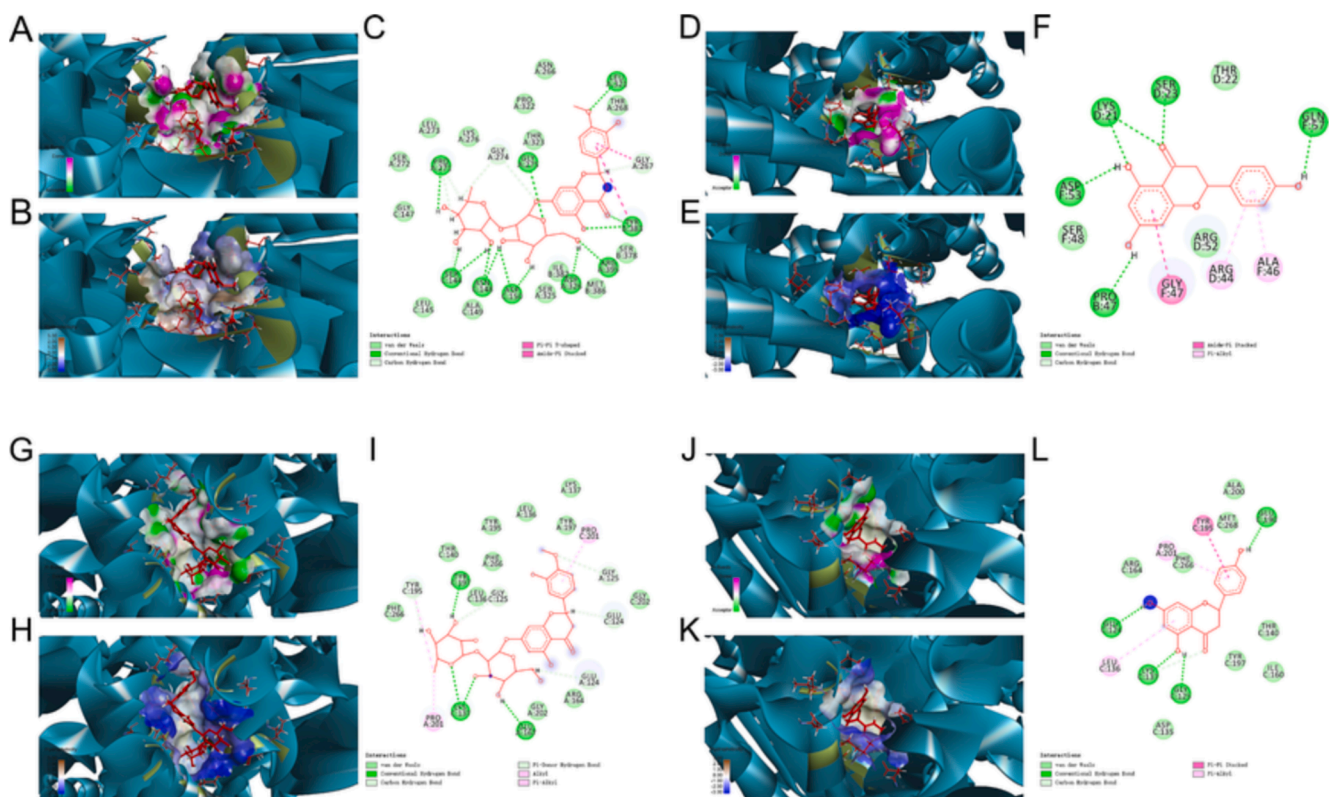


Fig. 5. Molecular docking analysis revealed the bond pattern of neohesperidin and naringenin with Caspase9 and Caspase3, respectively. (A-C) Molecular docking of neohesperidin and Caspase9, (D-F) Molecular docking of naringenin and Caspase9, (G-I) Molecular docking of neohesperidin and Caspase3, (J-L) Molecular docking of naringenin and Caspase3, (A, D, G, J): Areas of the donor and acceptor of hydrogen bond (H-bond). (B, E, H, K): Areas of hydrophobicity. (C, F, I, L): Two-dimensional patterns of the bond.

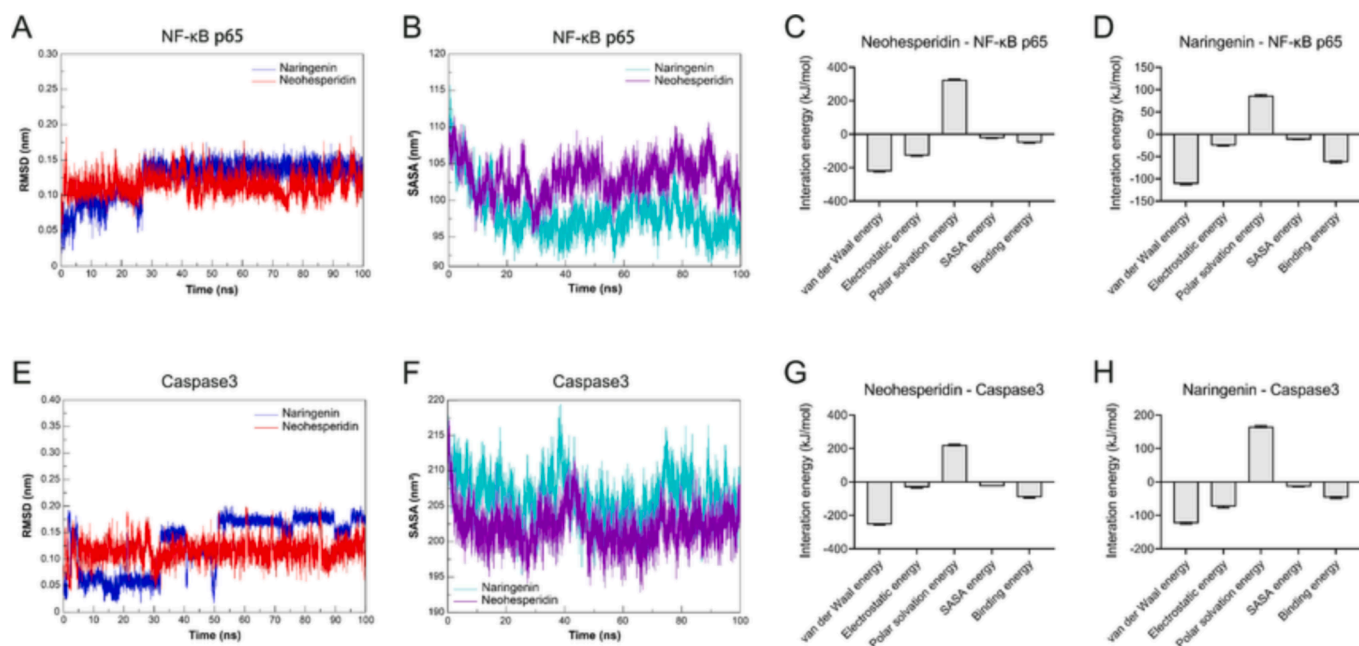


Fig. 6. Molecular dynamics simulations confirmed the stability of neohesperidin and naringenin with NF- κ B p65 and Caspase3 in the binding pocket, respectively. (A) RMSD analysis for NF- κ B p65 with neohesperidin and naringenin complexes. (B) The plot of SASA of NF- κ B p65 with neohesperidin and naringenin complexes. (C) Binding free energy decomposition of neohesperidin-NF- κ B p65 complex. (D) Binding free energy decomposition of naringenin-NF- κ B p65 complex. (E) RMSD analysis for Caspase3 with neohesperidin and naringenin complexes. (F) The plot of SASA of Caspase3 with neohesperidin and naringenin complexes. (G) Binding free energy decomposition of the neohesperidin-Caspase3 complex. (H) Binding free energy decomposition of the naringenin-Caspase3 complex.

converged values, the more structural stability. The neohesperidin-NF- κ B p65 system and naringenin-NF- κ B p65 system gradually stabilized in the 75 to 100 ns period with mean values of $206.3 \pm 2.970 \text{ nm}^2$ and $202.4 \pm 2.122 \text{ nm}^2$ (Fig. 6B), respectively. The results of the binding free energy analysis showed that the van der Waal energy between

neohesperidin and NF- κ B p65 was $-222.503 \pm 3.619 \text{ kJ/mol}$, the electrostatic energy was $-128.713 \pm 3.148 \text{ kJ/mol}$, the polar solvation energy was $325.487 \pm 3.635 \text{ kJ/mol}$, the SASA energy was $-25.258 \pm 0.310 \text{ kJ/mol}$, and the total binding energy was $-50.958 \pm 3.175 \text{ kJ}$ (Fig. 6C). By contrast, the van der Waal energy of naringenin with NF- κ B

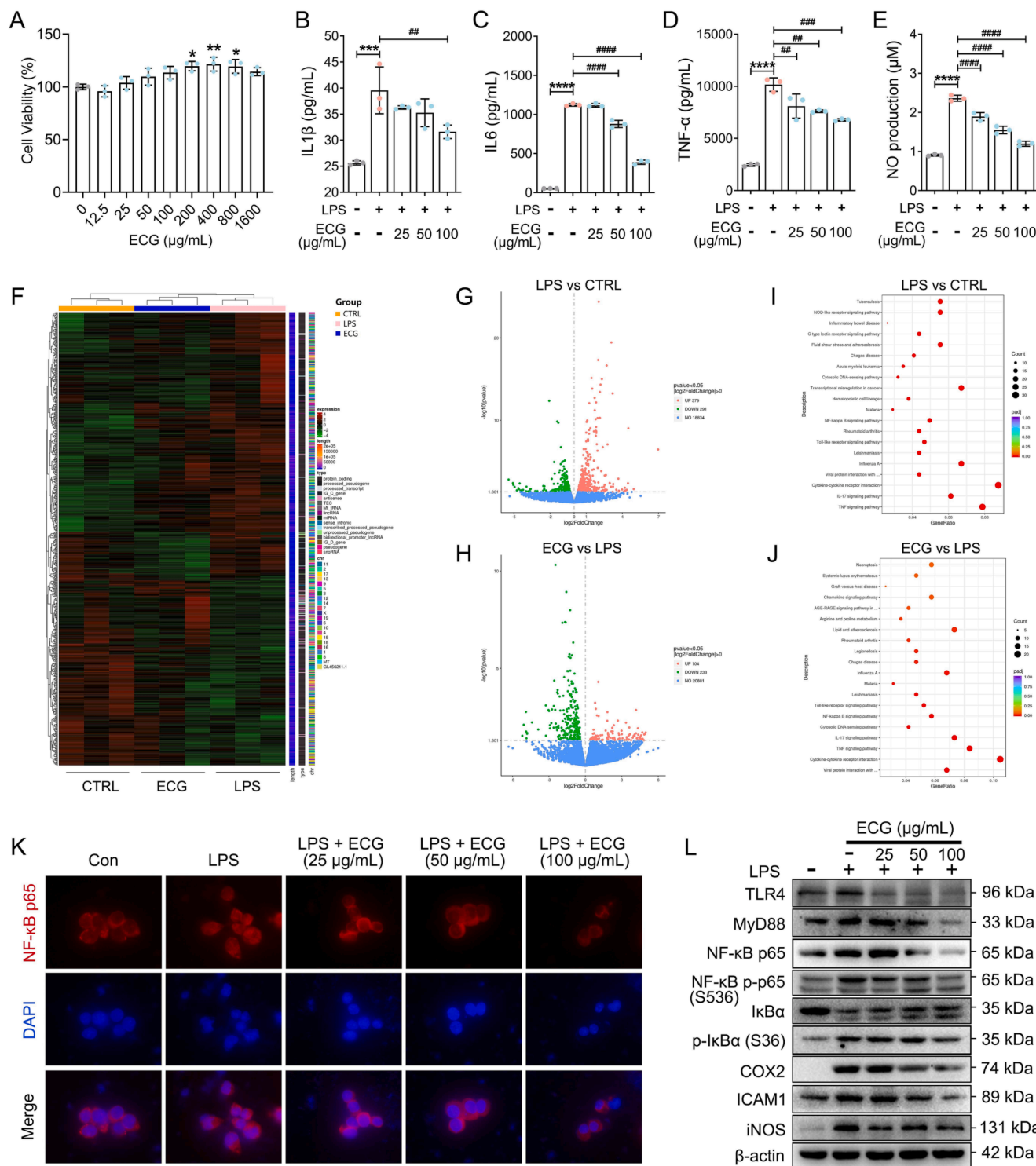


Fig. 7. ECG inhibited LPS-stimulated TLR4/MyD88/NF- κ B p65 signaling in RAW 264.7 cells. (A) Cell viability. IL1 β (B), IL6 (C), and TNF- α (D) levels in culture supernatants were measured using ELISA kits. (E) Production of NO. (F) The hierarchical clustering heat maps of DGEs ($n = 3$). (G) Volcano map of LPS vs. CTRL (Con). (H) Volcano map of ECG vs. LPS. (I) KEGG pathway analysis for DGEs of LPS vs. CTRL (Con). (J) KEGG pathway analysis for DGEs of ECG vs. LPS. (K) Representative images of immunofluorescence of NF- κ B p65. (L) Representative Western blots showing the proteins of TLR4, MyD88, NF- κ B p65, NF- κ B p-p65 (S536), I κ B α , p-I κ B α (S36), COX2, ICAM1, and iNOS changes and normalized to β -actin. Similar results were obtained from three independent experiments. Data are shown as the mean \pm SD. * $p < 0.05$, ** $p < 0.01$, *** $p < 0.001$, and **** $p < 0.0001$ vs. the control group. ## $p < 0.01$, ### $p < 0.001$, #### $p < 0.0001$ vs. the LPS group.

p65 was -111.626 ± 1.690 kJ/mol, the electrostatic energy was -25.214 ± 1.475 kJ/mol, the polar solvation energy was 86.682 ± 2.350 kJ/mol, the SASA energy was -12.275 ± 0.206 kJ/mol, and the total binding energy was -62.510 ± 2.533 kJ/mol (Fig. 6D). The main contribution of amino acid residues in the binding regions of neohesperidin and naringenin to the binding free energy of NF- κ B p65 were shown in Supplementary Table 14 and Supplementary Table 15.

As a crucial component of apoptosis, caspase3 is involved in the proteolytic cleavage of numerous essential proteins. (Fernandes-Alnemri et al., 1994). In the current study, the mean RMSD of the neohesperidin-Caspase3 system at equilibrium was 0.1352 ± 0.010 . Similarly, the mean RMSD of the naringenin-Caspase3 system at equilibrium was 0.1151 ± 0.016 (Fig. 6E). The RMSD value of the whole system converged, and the system reached equilibrium. Furthermore, the results of SASA for the neohesperidin-Caspase3 and naringenin-Caspase3 systems gradually stabilized in the 90—100 ns period with mean values of 96.02 ± 1.597 nm² and 102.2 ± 2.109 nm² (Fig. 6F), respectively. The results of the binding free energy analysis showed that the van der Waal energy between neohesperidin and Caspase3 was -255.197 ± 2.682 kJ/mol, the electrostatic energy was -31.387 ± 3.454 kJ/mol, the polar solvation energy was 211.44 ± 4.284 kJ/mol, the SASA energy was -26.469 ± 0.169 kJ/mol, and the total binding energy was -91.684 ± 3.950 kJ (Fig. 6G). Equally, the van der Waal energy of naringenin with Caspase3 was -123.763 ± 2.859 kJ/mol, the electrostatic energy was -74.308 ± 2.933 kJ/mol, the polar solvation energy was 165.957 ± 2.742 kJ/mol, the SASA energy was -14.316 ± 0.126 kJ/mol, and the total binding energy was -46.575 ± 2.933 kJ/mol (Fig. 6H). The main contribution of amino acid residues in the binding regions of neohesperidin and naringenin to the binding free energy of Caspase3 was shown in Supplementary Table 16 and Supplementary Table 17.

All of these MD simulations revealed that the active ingredients of ECG were stable in the binding pocket with NF- κ B p65 and Caspase3, indicating that neohesperidin and naringenin were capable of binding directly interacting with critical targets in the inflammatory response and apoptotic signaling to exert their anti-CB pharmacological effects. Notably, these findings were in line with the results of network pharmacological and molecular docking studies discussed above.

3.6. ECG inhibited LPS-stimulated NF- κ B signaling activation

Toll-like receptor 4 (TLR4), a macrophage LPS signaling receptor, cooperates with LY96 and CD14 to mediate the innate immune response and acts via MyD88, leading to NF- κ B activation, thereby triggering the release of various inflammatory mediators (Raetz and Whitfield, 2002), such as IL1 β , IL6, and TNF- α (Beutler and Cerami, 1988; Dinarello, 1991; Qu et al., 2020). Due to limitations in the establishment of animal models of CB, an *in vitro* LPS-induced RAW 264.7 macrophage inflammation model was used to investigate the anti-inflammatory mechanisms of ECG on CB in this study. As shown in Fig. 7A, ECG was not toxic to RAW264.7 cells but promoted cell proliferation above 200 μ g/mL according to CCK-8 results. Exposure to LPS resulted in significant production of IL1 β , IL6, TNF- α , and NO, while ECG pre-treatment significantly reduced those cytokines secretion (Fig. 7B-E). The transcriptome results showed that a total of 670 DEGs were screened in the LPS and CTRL (Con) comparison groups, of which 379 were up-regulated and 291 were down-regulated (Supplementary Table 18). Meanwhile, a total of 337 DEGs were screened between ECG and LPS groups, and among them, 104 were up-regulated and 233 were down-regulated (Fig. 7F-H, and Supplementary Table 19). By further KEGG analysis of these DEGs, the NF- κ B signaling pathway, the Toll-like receptor signaling pathway, the IL-17 signaling pathway, and the TNF signaling pathway were found to be closely related pathways, indicating that ECG may significantly inhibit the activation of inflammatory signaling in ameliorating the development of CB (Fig. 7I-J). Furthermore, immunofluorescence and immunoblotting results confirmed the

inhibition of TLR4/MyD88/NF κ B signaling by ECG and showed that ECG significantly inhibited NF- κ B p65 entry into the nucleus (Fig. 7K), down-regulated the expression of TLR4, MyD88, NF- κ B p65, NF- κ B p-p65 (S536), p-I κ B α (S36), COX2, ICAM1, and iNOS proteins and up-regulated the expression of I κ B α protein in LPS-induced RAW264.7 macrophages (Fig. 7L), suggesting that ECG could inhibit NF- κ B signaling transduction, and thus resist the onset and progression of inflammation closely related to CB.

3.7. ECG inhibited LPS-stimulated apoptosis

It is well known that activation of NF- κ B signaling has numerous been demonstrated to be associated with apoptosis (Khandelwal, 2011; Lawrence et al., 2001; Lo et al., 2011). The above studies demonstrated the significant inhibitory ability of ECG on NF- κ B signaling. To further explore the pharmacological mechanisms of ECG, Annexin V-FITC/PI staining and immunoblotting were carried out to study the effect of ECG on LPS-stimulated apoptosis in RAW264.7 cells. As expected, LPS stimulation of RAW264.7 macrophages resulted in significant apoptosis. Interestingly, pre-treatment with ECG suppressed this in a dose-dependent manner (Fig. 8A). Additionally, ECG significantly up-regulated the expression of anti-apoptotic protein Bcl-2 and down-regulated the expression of pro-apoptotic proteins including Bax, Caspase3, Caspase8, and Caspase9 (Fig. 8B), indicating that ECG played an essential role in the inflammatory response by inhibiting apoptosis.

4. Discussion

CB is a prevalent inflammatory disease of the respiratory system, and exposure to cigarette smoke could be its critical causative factor (Mallesker et al., 2020; Pelkonen et al., 2006), no matter due to active smoking or passive inhalation. As we all know, bacterial and viral infections are the typical reasons causing acute bronchitis, however, repeated exposure to infections is also a trigger for chronic bronchitis. The pathogenic feature of CB is characterized by overproduction and hypersecretion of goblet cell mucus. In response to harmful, infectious stimuli, epithelial cells lining the airways can release the inflammatory mediators' pro-inflammatory cytokines (Kim and Criner, 2013). Thus, one treatment option for CB is reducing mucus hypersecretion by controlling inflammation. ECG is an effective herbal medicine remedy that has been widely used to treat wind-cold coughs, itchy throats with profuse expectoration, nausea, vomiting, and epigastric distension brought on by improper diet. Clinical trials have demonstrated the significant efficacy of the TCM prescription "Juhong Pills" and "Juhong Capsules" with ECG as the monarch medicine in treating CB (Jiang et al., 1994; Xie et al., 2022). However, the pharmacological mechanisms of ECG in treating CB remain unclear.

In the present study, a network pharmacology-based strategy was proposed to investigate the potential molecular mechanisms of ECG in treating CB. Notably, 10 active ingredients of ECG and 46 overlap CB-related targets were screened out. Bioinformatics analysis showed that these targets were mostly implicated in the TNF signaling pathway, the IL-17 signaling pathway, and the PI3K/Akt signaling pathway, indicating active ingredients of ECG are crucial to the pathogenesis of CB.

To further explore the molecular mechanisms of ECG on CB, molecular docking techniques for computer-aided drug design were applied to resolve the interaction patterns between the screened ECG active ingredients and targets. Inflammation involves the sequential activation of signaling pathways that lead to the production of pro- and anti-inflammatory mediators (Lo et al., 2011). NF- κ B, a pivotal mediator of the inflammatory response, is triggered by MyD88 and TRIF-dependent pathways and regulates several aspects of innate and adaptive immune functions (Liu et al., 2017). The MyD88-dependent TLR pathway is essential for the inducible expression of pro-inflammatory cytokines (Yu et al., 2014). Our docking studies showed that neohesperidin, naringenin, and other active ingredients exhibited good binding activity

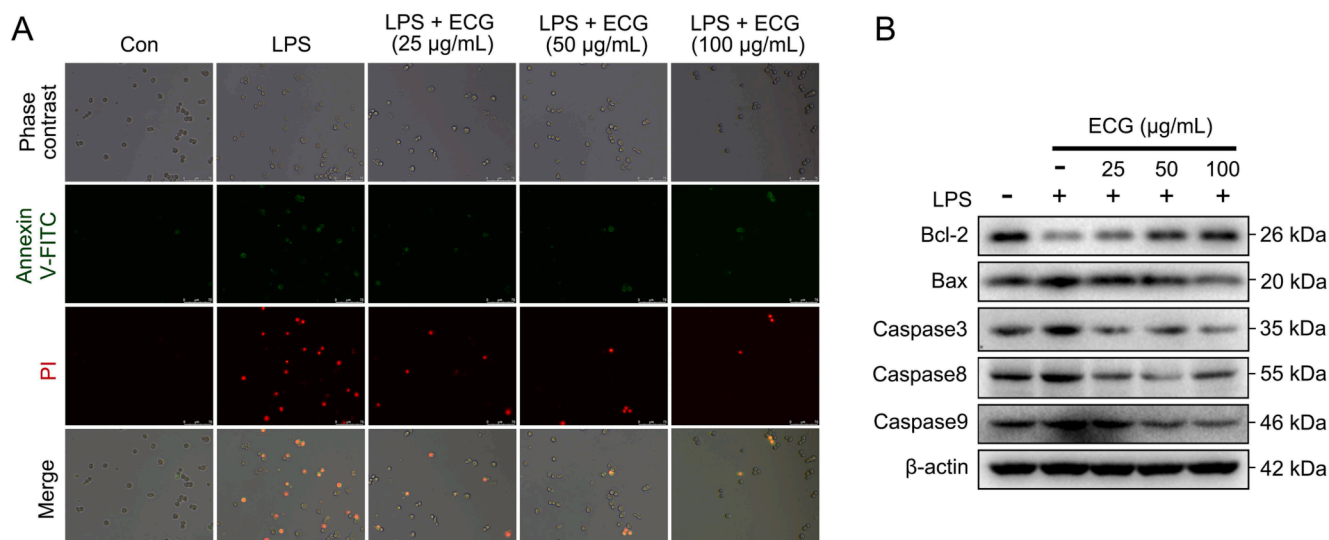


Fig. 8. ECG inhibited LPS-stimulated apoptosis in RAW 264.7 cells. (A) Cells were stained with Annexin V-FITC, and PI was analyzed by fluorescence microscope. (B) Representative Western blots showing the proteins of Bcl-2, Bax, Caspase3, Caspase8, and Caspase9 changes and normalized to β -actin. Similar results were obtained from three independent experiments.

with MyD88 and NF- κ B p65, respectively, suggesting that ECG active ingredients can act directly on critical targets of the inflammatory signaling pathway and thus affect the onset and progression of CB. Of note, the NF- κ B pathway is stimulated in response to cellular stress and it causes cytoplasmic relocalization of nucleophosmin which encourages apoptosis (Fan et al., 2008; Perkins and Gilmore, 2006; Radhakrishnan and Kamalakaran, 2006; Khandelwal et al., 2011). Similarly, neohesperidin, naringenin, and other active ingredients showed high affinity in the result of docking to the essential apoptosis proteins such as Caspase3 and Caspase9, indicating an important role of ECG in suppressing inflammatory responses and apoptosis with multiple active components, multiple targets, and multiple pathways. Furthermore, MD simulations showed that neohesperidin and naringenin were strongly stable in the binding pocket with NF- κ B p65 and Caspase3, suggesting ECG could mediate the TNF signaling pathway, the IL-17 signaling pathway, and apoptosis signaling pathway to exert anti-CB-pharmacological-effects.

Mucous metaplasia is the pathophysiological basis for CB. It is a process that mucus overproduces in response to inflammatory signals (Kim and Criner, 2013). LPS, a significant component of the external lipid membrane in Gram-negative bacteria, can activate innate immunity by recognizing pathogens through TLRs (Jeyaseelan et al., 2004). LPS-induced macrophage inflammation model *in vitro* has been widely used for drug development. The release of cytokines and inflammatory mediators such as IL6, TNF- α , iNOS, COX2, and ICAM1 through NF- κ B is mediated by MyD88, an essential adaptor molecule for most TLRs (Qu et al., 2020; Sugiyama et al., 2016). In the current study, due to limitations in the establishment of animal models of CB, the LPS-stimulated murine macrophage RAW 264.7 inflammatory model was used to investigate the anti-inflammation molecular mechanisms of ECG. As expected, ECG pro-treatment effectively decreased the release of IL1 β , IL6, TNF- α , and NO. Transcriptomics analysis showed that a total of 337 DEGs were screened after ECG treatment. Among them, 233 down-regulated DEGs were closely associated with the NF-kappa B signaling pathway, the Toll-like receptor signaling pathway, the IL-17 signaling pathway, and the TNF signaling pathway. Further molecular mechanism studies revealed that ECG significantly inhibited LPS-stimulated TLR4, MyD88, NF- κ B p65, NF- κ B p-p65 (S536), p-I κ B α (S36), COX2, ICAM1, and iNOS proteins expression, up-regulated I κ B α protein expression, reduced I κ B α dissociation, which in turn prevented NF- κ B p65 from entering the nucleus inducing the release of inflammatory cytokines

(Hoffmann et al., 2002; Hayden and Ghosh, 2008), This demonstrated the efficient anti-inflammatory capacity of ECG.

ECG significantly inhibited TLR4/MyD88/NF- κ B p65 signaling suggesting its decisive role in suppressing the onset and progression of inflammation. Studies have shown that activation of NF- κ B mediates apoptosis (Khandelwal, 2011; Lawrence et al., 2001; Lo et al., 2011). Cell survival requires active apoptosis inhibition by suppressing the expression of pro-apoptotic factors and up-regulated the expression of anti-apoptotic factors. In response to various apoptotic stimuli, the anti-apoptotic protein Bcl-2 exerts a survival function by inhibiting Caspase activity either by limiting cytochrome *c* released from the mitochondria or by connecting to the apoptosis-activating factor (Murphy et al., 2000). Conversely, Bax is a critical component in the apoptosis caused by mitochondrial stress (Wei et al., 2001). In response to apoptotic stimulation, Bax forms oligomers and its location is transferred from the cytosol to the mitochondrial membrane (Jürgensmeier et al., 1998), and increases membrane permeability, which causes the release of cytochrome *C* from mitochondria and the activation of Caspase9 and Caspase-activated pathways for apoptosis (Narita et al., 1998; Marzo et al., 1998). Notably, in the current study, ECG pro-treatment markedly up-regulated Bcl-2 protein expression, and down-regulated LPS-stimulated Bax, Caspase3, Caspase8, and Caspase9 protein expression, demonstrating a significant ability to inhibit apoptosis, which was a pharmacological mechanism closely related to the ECG treatment of CB.

5. Conclusion

Collectively, this study systematically investigated potential pharmacological mechanisms of the active ingredients of ECG in treating CB. Our findings suggested that ECG might be involved in the suppression of TLR4/MyD88/NF- κ B p65-mediated inflammatory response and Bcl-2/Bax/Caspase3-mediated apoptosis. The resulting findings reveal the potential mechanisms of ECG for the treatment of CB and provide a scientific basis for its development and clinical application.

Author contribution

Jiawen Huang, Xiaoling Shen, and Zhuohui Luo contributed to the design and concept of the study. Jiawen Huang, Zaibin Xu, Jiayu Li, Xinqian He, and Xinan Huang analyzed and interpreted the data. Jiawen Huang, Xiaoling Shen, and Zhuohui Luo wrote the manuscript.

Declaration of Competing Interest

The authors declare that they have no known competing financial interests or personal relationships that could have appeared to influence the work reported in this paper.

Acknowledgements

This work was financially supported by the China Postdoctoral Science Foundation (No. 2021M701026), the National Natural Science Foundation of China (82304826, 82360882), and projects of the Guangzhou University of Chinese Medicine (No. E2-6216-212-453-001, 41-2601-22-414-001Z57). The work also got the support of Novogene Co., Ltd. (Beijing, China) in sequencing.

Appendix A. Supplementary material

Supplementary data to this article can be found online at <https://doi.org/10.1016/j.arabjc.2023.105428>.

References

- Amberger, J.S., Bocchini, C.A., Schiettecatte, F., Scott, A.F., Hamosh, A., 2015. OMIM.org: Online Mendelian Inheritance in Man (OMIM®), an online catalog of human genes and genetic disorders. *Nucleic Acids Res* 43 (Database issue), D789-D798.
- Anonymou, 1965. Definition and classification of chronic bronchitis for clinical and epidemiological purposes. A report to the Medical Research Council by their Committee on the Aetiology of Chronic Bronchitis. *Lancet* 1 (7389), 775-779.
- Bauerle, P.A., Baltimore, D., 1996. NF-kappa B: ten years after. *Cell* 87 (1), 13-20.
- Bauerle, P.A., Henkel, T., 1994. Function and activation of NF-kappa B in the immune system. *Annu. Rev. Immunol.* 12, 141-179.
- Beutler, B., Cerami, A., 1988. Tumor necrosis, cachexia, shock, and inflammation: a common mediator. *Annu. Rev. Biochem.* 57, 505-518.
- Burley, S.K., Berman, H.M., Bhikadiya, C., Bi, C., Chen, L., Di Costanzo, L., Christie, C., Dalenberg, K., Duarte, J.M., Dutta, S., Feng, Z., Ghosh, S., Goodsell, D.S., Green, R. K., Guranovic, V., Guzenko, D., Hudson, B.P., Kalro, T., Liang, Y., Lowe, R., Namkoong, H., Peisach, E., Periskova, I., Prlc, A., Randle, C., Rose, A., Rose, P., Sala, R., Sekharan, M., Shao, C., Tan, L., Tao, Y.P., Valasatava, Y., Voigt, M., Westbrook, J., Woo, J., Yang, H., Young, J., Zhuravleva, M., Zardecki, C., 2019. RCSB Protein Data Bank: biological macromolecular structures enabling research and education in fundamental biology, biomedicine, biotechnology and energy. *Nucleic Acids Res.* 47 (D1), D464-D474.
- Cameron, A.M., Lawless, S.J., Pearce, E.J., 2016. Metabolism and acetylation in innate immune cell function and fate. *Semin. Immunol.* 28 (5), 408-416.
- Chen, Z., Lin, L., 2004. Study on coumarin compounds from *Exocarpium Citri Grandis*. *Zhong Yao Cai* 27 (8), 577-578.
- Dinarello, C.A., 1991. Interleukin-1 and interleukin-1 antagonism. *Blood* 77 (8), 1627-1652.
- Fan, Y., Dutta, J., Gupta, N., Fan, G., Gélinas, C., 2008. Regulation of programmed cell death by NF-kappaB and its role in tumorigenesis and therapy. *Adv. Exp. Med. Biol.* 615, 223-250.
- Fernandes-Alnemri, T., Litwack, G., Alnemri, E.S., 1994. CPP32, a novel human apoptotic protein with homology to Caenorhabditis elegans cell death protein Ced-3 and mammalian interleukin-1 beta-converting enzyme. *J. Biol. Chem.* 269 (49), 30761-30764.
- Hayden, M.S., Ghosh, S., 2008. Shared principles in NF-kappaB signaling. *Cell* 132 (3), 344-362.
- Hoffmann, A., Levchenko, A., Scott, M.L., Baltimore, D., 2002. The IkkappaB-NF-kappaB signaling module: temporal control and selective gene activation. *Science* 298 (5596), 1241-1245.
- Hopkins, A.L., 2007. Network pharmacology. *Nat. Biotechnol.* 25 (10), 1110-1111.
- Huang, W.D., Sherman, B.T., Lempicki, R.A., 2009. Systematic and integrative analysis of large gene lists using DAVID bioinformatics resources. *Nat. Protoc.* 4 (1), 44-57.
- Jeyaseelan, S., Chu, H.W., Young, S.K., Worthen, G.S., 2004. Transcriptional profiling of lipopolysaccharide-induced acute lung injury. *Infect. Immun.* 72 (12), 7247-7256.
- Jiang, J.P., Shan, L.T., Chen, Z.Y., Xu, H.S., Wang, J.P., Liu, Y.W., Xiong, Y.K., 2014. Evaluation of antioxidant-associated efficacy of flavonoid extracts from a traditional Chinese medicine Hua Ju Hong (peels of Citrus grandis (L.) Osbeck). *J. Ethnopharmacol.* 158, 325-330.
- Jiang, K., Song, Q., Wang, L., Xie, T.Z., Wu, X., Wang, P., Yin, G., Ye, W.C., Wang, T.J., 2014. Antitussive, expectorant and anti-inflammatory activities of different extracts from *Exocarpium Citri grandis*. *J. Ethnopharmacol.* 156, 97-101.
- Jiang, S.S., Wang, X.P., Yang, Y.G., 1994. Clinical and experimental study on the treatment of chronic bronchitis (phlegm-heat type) with Juhong tea bag. *Hum. J. Trad. Chinese Med.* 10 (1), 44-45.
- Jürgensmeier, J.M., Xie, Z., Deveraux, Q., Ellerby, L., Brédesein, D., Reed, J.C., 1998. Bax directly induces release of cytochrome c from isolated mitochondria. *PNAS* 95 (9), 4997-5002.
- Khandelwal, N., Simpson, J., Taylor, G., Rafique, S., Whitehouse, A., Hiscox, J., Stark, L. A., 2011. Nucleolar NF-κB/RelA mediates apoptosis by causing cytoplasmic relocalization of nucleophosmin. *Cell Death Differ.* 18 (12), 1889-1903.
- Kim, V., Criner, G.J., 2013. Chronic bronchitis and chronic obstructive pulmonary disease. *Am. J. Respir. Crit. Care Med.* 187 (3), 228-237.
- Kim, J., So, S., Lee, H.J., Park, J.C., Kim, J.J., Lee, H., 2013. DigSee: Disease gene search engine with evidence sentences (version cancer). *Nucleic Acids Res* 41 (Web Server issue), W510-W517.
- Kong, F.S., Ding, Z.D., Zhang, K., Duan, W.J., Qin, Y.R., Su, Z.P., Bi, Y.G., 2022. Optimization of extraction flavonoids from *Exocarpium Citri Grandis* and evaluation its hypoglycemic and hypolipidemic activities. *J. Ethnopharmacol.* 262, 113178.
- Kumari, R., Kumar, R., Open Source Drug Discovery Consortium, Lynn, A., 2014. g_mmpbsa—a GROMACS tool for high-throughput MM-PBSA calculations. *J. Chem. Inf. Model* 54 (7), 1951-1962.
- Lawrence, T., Gilroy, D.W., Colville-Nash, P.R., Willoughby, D.A., 2001. Possible new role for NF-kappaB in the resolution of inflammation. *Nat. Med.* 7 (12), 1291-1297.
- Li, H.J., Liu, S.B., Du, Y.Q., Tan, J., Luo, J.Z., Sun, Y.L., 2020. Hub proteins involved in RAW 264.7 macrophages exposed to direct current electric field. *Int. J. Mol. Sci.* 21 (12), 4505.
- Li, P.B., Ma, Y., Wang, Y.G., Su, W.W., 2006. Experimental studies on antitussive, expectorant and antiasthmatic effects of extract from *Citrus grandis* var. tomentosa. *Zhongguo Zhong Yao Za Zhi* 31 (16), 1350-1352.
- Liu, G.X., Li, S.Y., Zhang, N., Wei, N.M., Wang, M.X., Liu, J., Xu, Y., Li, Y.N., Sun, Q.Q., Li, Y.X., Li, F., Yu, P.H., Liu, M.Y., Wang, Y.P., Zhai, H.Q., Wang, Y.Y., 2022. Sequential grade evaluation method exploration of Exocarpium Citri Grandis (Huajuhong) decoction pieces based on "network prediction → grading quantization → efficacy validation". *J. Ethnopharmacol.* 291, 115149.
- Liu, Z.W., Luo, Z.H., Meng, Q.Q., Zhong, P.C., Hu, Y.J., Shen, X.L., 2020. Network pharmacology-based investigation on the mechanisms of action of *Morinda officinalis* How. in the treatment of osteoporosis. *Comput. Biol. Med.* 127, 104074.
- Liu, T., Zhang, L.Y., Joo, D.H., Sun, S.C., 2017. NF-κB signaling in inflammation. *Signal Transduct. Target. Ther.* 2, 17023.
- Liu, M.J., Zhang, G.H., Zheng, C.G., Song, M., Liu, F.L., Huang, X.T., Bai, S.S., Huang, X. A., Lin, C.Z., Zhu, C.C., Hu, Y.J., Mi, S.Q., Liu, C.H., 2018. Activating the pregnane X receptor by imperatorin attenuates dextran sulphate sodium-induced colitis in mice. *Br. J. Pharmacol.* 175 (17), 3563-3580.
- Lo, S.Z.Y., Steer, J.H., Joyce, D.A., 2011. TNF-α renders macrophages resistant to a range of cancer chemotherapeutic agents through NF-κB-mediated antagonism of apoptosis signaling. *Cancer Lett.* 307 (1), 80-92.
- Luo, Z.H., Huang, J.W., Li, E.N., He, X.Q., Meng, Q.Q., Huang, X.N., Shen, X.L., Yan, C.K., 2022. An integrated pharmacology-based strategy to investigate the potential mechanism of Xiebai San in treating pediatric pneumonia. *Front. Pharmacol.* 13, 784729.
- Malesker, M.A., Callahan-Lyon, P., Madison, J.M., Ireland, B., Irwin, R.S., 2020. Chronic cough due to stable chronic bronchitis: CHEST expert panel report. *Chest* 158 (2), 705-718.
- Marzo, I., Brenner, C., Zamzami, N., Jürgensmeier, J.M., Susin, S.A., Vieira, H.L., Prévost, M.C., Xie, Z., Matsuyama, S., Reed, J.C., Kroemer, G., 1998. Bax and adenine nucleotide translocator cooperate in the mitochondrial control of apoptosis. *Science* 281 (5385), 2027-2031.
- Murphy, K.M., Ranganathan, V., Farnsworth, M.L., Kavallaris, M., Lock, R.B., 2000. Bcl-2 inhibits Bax translocation from cytosol to mitochondria during drug-induced apoptosis of human tumor cells. *Cell Death Differ.* 7 (1), 102-111.
- Narita, M., Shimizu, S., Ito, T., Chittenden, T., Lutz, R.J., Matsuda, H., Tsujimoto, Y., 1998. Bax interacts with the permeability transition pore to induce permeability transition and cytochrome c release in isolated mitochondria. *PNAS* 95 (25), 14681-14686.
- Pelkonen, M., Notkola, I.L., Nissinen, A., Tukiainen, H., Koskela, H., 2006. Thirty-year cumulative incidence of chronic bronchitis and COPD in relation to 30-year pulmonary function and 40-year mortality: a follow-up in middle-aged rural men. *Chest* 130 (4), 1129-1137.
- Perkins, N.D., Gilmore, T.D., 2006. Good cop, bad cop: the different faces of NF-kappaB. *Cell Death Differ.* 13 (5), 759-772.
- Qu, Z., Chen, Y., Luo, Z.H., Shen, X.L., Hu, Y.J., 2020. 7-methoxyflavone alleviates neuroinflammation in lipopolysaccharide-stimulated microglial cells by inhibiting TLR4/MyD88/MAPK signaling and activating the Nrf2/NQO-1 pathway. *J. Pharm. Pharmacol.* 72 (3), 385-395.
- Radhakrishnan, S.K., Kamalakaran, S., 2006. Pro-apoptotic role of NF-kappaB: implications for cancer therapy. *Biochim. Biophys. Acta* 1766 (1), 53-62.
- Raetz, C.R., Whitfield, C., 2002. Lipopolysaccharide endotoxins. *Annu. Rev. Biochem.* 71, 635-700.
- Rebhan, M., Chalifa-Caspi, V., Prilusky, J., Lancet, D., 1997. GeneCards: integrating information about genes, proteins and diseases. *Trends Genet.* 13 (4), 163.
- Ru, J.L., Li, P., Wang, J.N., Zhou, W., Li, B.H., Huang, C., Li, P.D., Guo, Z.H., Tao, W.Y., Yang, Y.F., Xu, X., Li, Y., Wang, Y.H., Yang, L., 2014. TCMSP: a database of systems pharmacology for drug discovery from herbal medicines. *J. Cheminform.* 6, 13.
- Sugiyama, K., Muroi, M., Kinoshita, M., Hamada, O., Minai, Y., Sugita-Konishi, Y., Kamata, Y., Tanamoto, K., 2016. NF-κB activation via MyD88-dependent Toll-like receptor signaling is inhibited by trichothecene mycotoxin deoxynivalenol. *J. Toxicol. Sci.* 41 (2), 273-279.
- Szklarczyk, D., Morris, J.H., Cook, H., Kuhn, M., Wyder, S., Simonovic, M., Santos, A., Doncheva, N.T., Roth, A., Bork, P., Jensen, L.J., von Mering, C., 2017. The STRING database in 2017: quality-controlled protein-protein association networks, made broadly accessible. *Nucleic Acids Res.* 45 (D1), D362-D368.

- Wang, Y., Xiao, J., Suzek, T.O., Zhang, J., Wang, J., Bryant, S.H., 2009. PubChem: a public information system for analyzing bioactivities of small molecules. *Nucleic Acids Res* 37 (Web Server issue), W623-W633.
- Wei, M.C., Zong, W.X., Cheng, E.H., Lindsten, T., Panoutsakopoulou, V., Ross, A.J., Roth, K.A., MacGregor, G.R., Thompson, C.B., Korsmeyer, S.J., 2001. Proapoptotic BAX and BAK: a requisite gateway to mitochondrial dysfunction and death. *Science* 292 (5517), 727-730.
- Wishart, D.S., Knox, C., Guo, A.C., Cheng, D., Shrivastava, S., Tzur, D., Gautam, B., Hassanali, M., 2008. DrugBank: a knowledgebase for drugs, drug actions and drug targets. *Nucleic Acids Res* 36 (Database issue), D901-D906.
- Xie, B., Lu, Y.Y., Luo, Z.H., Qu, Z., Zheng, C.G., Huang, X.A., Zhou, H.Y., Hu, Y.J., Shen, X.L., 2019. Tenacigenin B ester derivatives from *Marsdenia tenacissima* actively inhibited CYP3A4 and enhanced in vivo antitumor activity of paclitaxel. *J. Ethnopharmacol.* 235, 309-319.
- Xie, L.J., Miu, K.Y., 2022. Clinical study on juhong capsules combined with Asmeton for acute attack of chronic bronchitis. *New Chinese Med.* 54 (16), 73-77.
- Yu, M., Zhou, H., Zhao, J., Xiao, N., Roychowdhury, S., Schmitt, D., Hu, B., Ransohoff, R. M., Harding, C.V., Hise, A.G., Hazen, S.L., DeFranco, A.L., Fox, P.L., Morton, R.E., Dicorleto, P.E., Febbraio, M., Nagy, L.E., Smith, J.D., Wang, J.A., Li, X., 2014. MyD88-dependent interplay between myeloid and endothelial cells in the initiation and progression of obesity-associated inflammatory diseases. *J. Exp. Med.* 211 (5), 887-907.
- Zhong, C.C., Wu, M.H., Yu, P.H., Li, F., Zhang, Y., Ma, Z.G., Xie, C.J., Cao, H., 2021. Herbalogical study on historical evolution of collection, processing and efficacy of *Citri Exocarpium Rubrum* and *Citri Grandis Exocarpium*. *Zhongguo Zhong Yao Za Zhi* 46 (18), 4865-4874.
- Zhu, Z.T., Wu, H., Su, W.W., Shi, R., Li, P.L., Liao, Y., Wang, Y.G., Li, P.B., 2019. Effects of total flavonoids from *Exocarpium Citri Grandis* on air pollution particle-induced pulmonary inflammation and oxidative stress in mice. *J. Food Sci.* 84 (12), 3843-3849.